14th Australasian Fluid Mechanics Conference
Adelaide University, Adelaide, Australia
10-14 December 2001

Three-dimensional modelling of a tsunami interacting with real topographical coastline using Smoothed Particle Hydrodynamics

François Debroux, Mahesh Prakash and Paul Cleary

CSIRO Mathematical and Information Sciences
Private Bag 10, Clayton South, VIC 3169, AUSTRALIA

Abstract

This paper presents the simulation of a tsunami wave interacting with a section of real coastline adapted from the US Geological Survey (USGS). The full Navier-Stokes equations are solved using the Smoothed Particle Hydrodynamics (SPH) method. Since the SPH method is mesh free it is well suited to simulating complex free-surface flows of this kind involving wave propagation, splashing, wave refraction and break up. The full three dimensional nature of the simulation allows important features such as the differential breaking of the wave due to variations in the sea bed level, preferential inundation of exposed coastal features and wave reflection and refraction. The paper demonstrates the ability of the SPH method to handle these large geophysical phenomena having length scales of the order of kilometres and to be able to predict information of importance for coastal defence.

Introduction

A tsunami is a series of waves generated in a body of water by an impulsive disturbance that vertically displaces the water column. Earthquakes, landslides, volcanic eruptions and explosions can generate tsunamis. Tsunamis can savagely attack coastlines, causing devastating loss of life and property damage. The extent of the damage depends on the strength of the wave generated by the tsunami and the location of wave impact. Thus, the prediction of these waves can prove to be extremely useful in minimising the loss of life and property.

In the past, simulations of tsunamis were carried out, by using the shallow water equations, which basically represent conservation of mass and momentum of a layer of water. Typical simulations of this kind are reported in [1, 2, 3]. All such simulations have been carried out in one or two-dimensions using a grid based finite difference or finite element method. Thus it becomes impossible to resolve three-dimensional features, which can be important in many geophysical flows. In [1] the tsunami was generated by an earthquake, which affected the western coast of Puerto Rico in 1918. The model results were compared with the observed run-up values, estimated to be a maximum of 6 metres above sea level. In [2] the tsunami was caused by an earthquake in Southern Italy in 1908. In this case the run-up was as high as 10 metres above sea level. In [3] the tsunami was hypothetically assumed to be caused by the sector collapse of a volcanic eruption in Stromboli, Italy. In all reported tsunami incidents, waves travel around the shore, due to strong wave refraction affecting even the coast opposite the source and cause enormous damage to life and property.

Smoothed Particle Hydrodynamics (SPH) was originally developed in the 1970's to solve compressible astrophysical problems [4]. Many applications involving free surface flows have been solved using the SPH method since then. Some examples include bursting of a dam and generation of a wave in two dimensions [5] and high pressure and gravity die-casting [6,7]. The two-dimensional wave phenomenon is handled extremely well by the SPH method [5]. Since a real tsunami is essentially a series of three-dimensional waves generated by different sources the problem was thought to be a natural candidate for the SPH method. The mesh free nature of the SPH method is well suited for simulating free-surface flows of the present kind involving splashing, wave refraction and break up.

The SPH methodology

A brief summary of the SPH method is presented here. For more comprehensive details please refer to [8,9]. The interpolated value of a function A at any position $\mathbf{r}$ can be expressed using SPH smoothing as:

$$A(\mathbf{r}) = \sum_b m_b \frac{A_b}{\rho_b} W(\mathbf{r} - \mathbf{r}_b, h) \qquad (1)$$

where m_b and ρ_b are the mass and density of particle b and the sum is over all particles b within a radius 2h of $\mathbf{r}$. Here $W(\mathbf{r},h)$ is a C^2 spline based interpolation or smoothing kernel with radius 2h, that approximates the shape of a Gaussian function but has compact support. The gradient of the function A is given by differentiating the interpolation equation (1) to give:

$$\nabla A(\mathbf{r}) = \sum_b m_b \frac{A_b}{\rho_b} \nabla W(\mathbf{r} - \mathbf{r}_b, h) \qquad (2)$$

Using these interpolation formulae and suitable finite difference approximations for second order derivatives, one is able to convert parabolic partial differential equations into ordinary differential equations for the motion of the particles and the rates of change of their properties.

Continuity equation:

From Monaghan [8], our preferred form of the SPH continuity equation is:

$$\frac{d\rho_a}{dt} = \sum_b m_b (\mathbf{v}_a - \mathbf{v}_b) \nabla W_{ab} \qquad (3)$$

where ρ_a is the density of particle a with velocity $\mathbf{v}_a$ and m_b is the mass of particle b. We denote the position vector from particle b to particle a by $\mathbf{r}_{ab} = \mathbf{r}_a - \mathbf{r}_b$ and let $W_{ab} = W(\mathbf{r}_{ab}, h)$ be the interpolation kernel with smoothing length h evaluated for the distance $|\mathbf{r}_{ab}|$.

This form of the continuity equation is Galilean invariant (since the positions and velocities appear only as differences), has good numerical conservation properties and is not affected by free surfaces or density discontinuities. The use of this form of the continuity equation is very important for predicting free surface flows of the present kind.

Momentum equation:

The SPH momentum equation used here is:

$$\frac{d\mathbf{v}_a}{dt} = \mathbf{g} - \sum_b m_b \left[\left(\frac{P_b}{\rho_b^2} + \frac{P_a}{\rho_a^2} \right) - \frac{\xi}{\rho_a \rho_b} \frac{4\mu_a \mu_b}{(\mu_a + \mu_b)} \frac{\mathbf{v}_{ab} \mathbf{r}_{ab}}{\mathbf{r}_{ab}^2 + \eta^2} \right] \nabla_a W_{ab} \quad (4)$$

where P_a and μ_a are pressure and viscosity of particle a and $\mathbf{v}_{ab} = \mathbf{v}_a - \mathbf{v}_b$. Here ξ is a factor associated with the viscous term [10], η is a small parameter used to smooth out the singularity at $\mathbf{r}_{ab} = 0$ and $\mathbf{g}$ is the gravity vector.

The first two terms involving the pressure correspond to the pressure gradient term of the Navier-Stokes equation. The next term involving viscosities is the Newtonian viscous stress term. This form ensures that stress is automatically continuous across material interfaces and allows the viscosity to be variable or discontinuous.

Equation of state:

Since the SPH method used here is quasi-compressible one needs to use an equation of state, giving the relationship between particle density and fluid pressure. This relationship is given by the expression:

$$P = P_0 \left[\left(\frac{\rho}{\rho_0} \right)^{\gamma} - 1 \right] \quad (5)$$

where P_0 is the magnitude of the pressure and ρ_0 is the reference density. For water and similar fluids $\gamma = 7$ is normally used [5]. This pressure is then used in the SPH momentum equation (4) to give the particle motion. The pressure scale factor P_0 is given by:

$$\frac{\gamma P_0}{\rho_0} = 100 V^2 = c_s^2 \quad (6)$$

where V is the characteristic or maximum fluid velocity. This ensures that the density variation is less than 1% and the flow can be regarded as incompressible.

Setting up the simulations

Simulations of a tsunami wave were carried out using real topography obtained from the US Geological Survey (USGS) website [11] shown in figure 1.

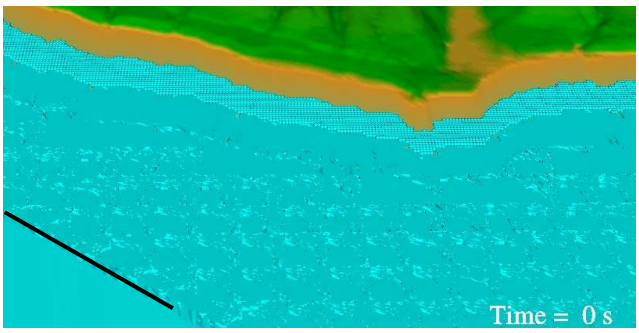

Figure 1. Digital Elevation Model of a section of coastal California and adjoining ocean obtained from USGS. Sections coloured blue (or the lighter shade in black and white) represent the ocean made up of SPH fluid particles.

The topography used was that of a section of coast near the Triunfo Pass located in the state of California in the US. Since data from a real tsunami affected region was not available, the above topography was used as a typical example. The topographic data was in the form of a Digital Elevation Model (DEM). A DEM is a digital file consisting of terrain elevations for ground positions at regularly spaced horizontal intervals. This data was used to generate boundary particles with an interpolation length in the range of 10.0 m. Fluid particles (the section coloured in blue or the lighter shade in black and white) were set up on a portion of the topography as shown in figure 1 to create the ocean. The ocean bed is sloped with the depth of water increasing with distance from the coast. The interpolation length of the fluid particles was fixed at 13.0 m. This ensured that the fluid particles would not penetrate the boundary in regions where the topography is too steep and the boundary particle interpolation length is significantly greater than 10.0 m. The tsunami waves were generated by a wave-maker. This is a vertical surface that moves horizontally with a sinusoidal motion. The thick line in the ocean in figure 1 shows the position of the wave-maker. The velocity of the wave-maker, v, varies according to the following equation:

$$v = v_{\max} \sin\left(\frac{\pi}{2} f t \right) \quad (7)$$

where $v_{max} = 180$ m/s is the maximum velocity of the piston,
f = 0.2 is a parameter by which the frequency of the piston motion can be controlled and
t = time in seconds.

The wave-maker has a zero velocity at the beginning of the simulation, reaches a maximum of 180 m/s 5 seconds into the simulation and falls back to zero after 10 seconds. This is a 3D analogy of the 2D wave-maker simulated in [5]. The movement of the piston is stopped after 10 seconds. The simulation continues for a period of 200 seconds allowing the propagation of the wave and its flow over the coastal terrain. The total number of fluid particles used in the simulation was approximately 140,000.

Results and Discussion

The ocean at rest and the position of the wave-maker is shown in figure 1 at time t = 0 s. When the wave-maker starts pushing the water according to the motion specified by equation (7) towards the shore, a wave is generated. Having completed one half of a sinusoidal cycle, the wave-maker stops after 10 s and the wave moves towards the shore.

The wave motion is shown in Figure 2. After 20 s (figure 2a) the wave is approaching the shore. After 50 s (figure 2b) the wave reaches the shore with considerable force, completely submerges the beach and coastal plane, and begins to inundate parts of the mountainous terrain behind - especially on the left of the coastline. Observe that the water has just begun flooding the valley between the mountains on the right of figure 2b. At 70 s, figure 2c, the water starts receding from the left of the coastline after striking the steep mountain slopes. Parts of the coastal plane are now exposed. Water is also flowing back down through the minor valleys on the left side. A substantial amount of water has now flowed into the main valley between the two mountains. Any man-made structure in such a region would have a high probability of severe damage caused by the intruding wave. In figure 2d, at 90 s, the water is still seen to be receding from the left of the coastline with significant amounts of the coastal plane now exposed. However, strong flows up into the central valley and onto the coastline on the right can be observed. This highlights the differences in inundation timing along the coast that occur when the angle of the incident wave and the coastal topography are considered. At 120 s, figure 2e shows the water receding from the right side of the coastline. In figure 2f (after 140 s) the wave has receded considerably from the right hand side shore but a secondary wave is now inundating the left part of the coastline. The progress of the secondary wave is shown in figures 2g and 2h, (160 s and 180 s respectively). This wave has a much lower intensity than the primary wave and is focused on the middle of the shoreline. Meanwhile the flooded central valley continues to drain. This shows that the time spent underwater by inland topography can be significantly greater than the time required for a tsunami to inundate it. Finally at 200 s (figure 2i) the wave has again receded from the left hand side

of the shore and a minor wave is flowing over the right side of the coast.

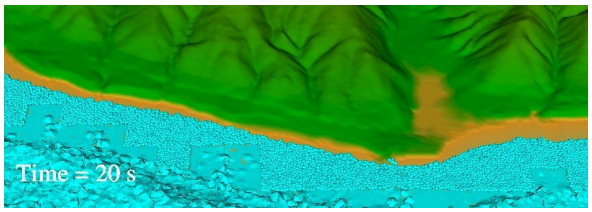

(a)

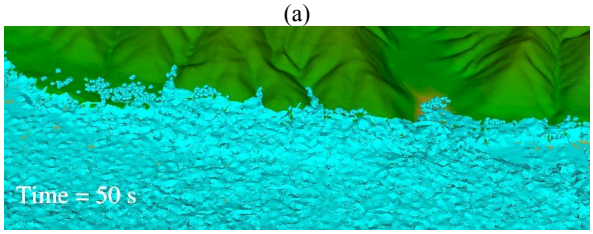

(b)

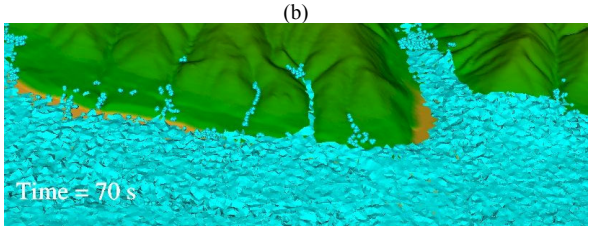

(c)

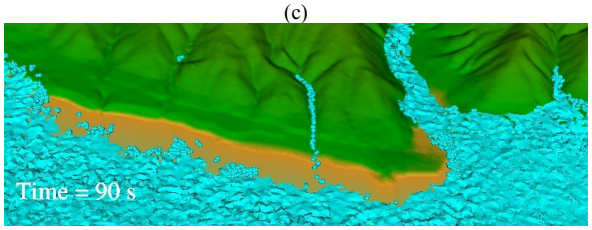

(d)

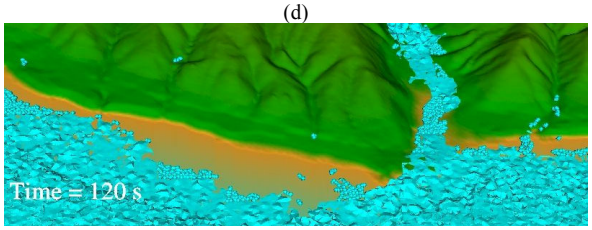

(e)

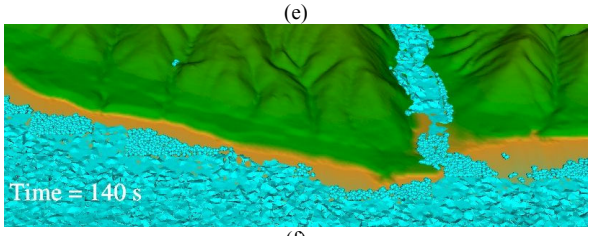

(f)

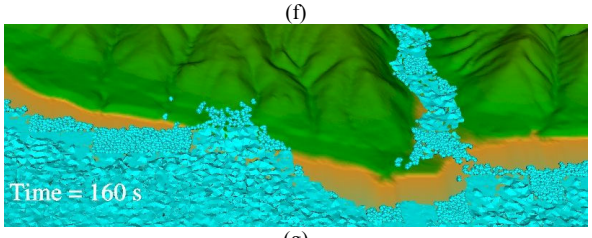

(g)

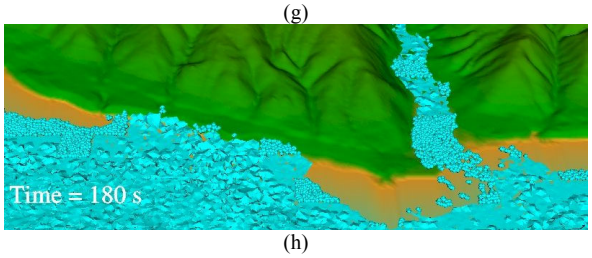

(h)

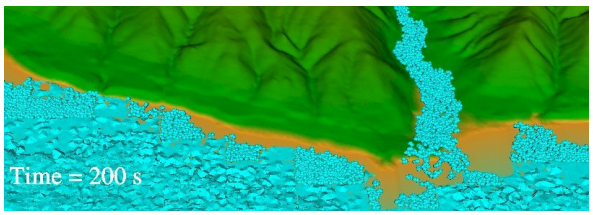

(i)

Figure 2. Front view snapshots of the predicted inundation of the coastline by the tsunami wave at different times

Figure 3 shows some snapshots of the tsunami wave viewed from the mountain range. Initially (figure 1) about 300 m of the beach (normal to the coastline) is exposed. After 40 s, figure 3a, a significant portion of the beach has been inundated by the wave. One can see a preferential movement of the wave towards the right of the coastline. At 60 s, figure3b gives a clearer view of the water rising onto and inundating the coastline, particularly the major central valley between and two minor valleys on the right. In figure 3c (at 80s) the wave starts receding from the right but moves further onto the coast on the left and deeper into the central valley. At 110 s, figure 3d, the wave has receded further away from the right side coastline and has also started receding from the left. At 150 s, figure 3e, one can see the secondary wave striking the coastline on the right.

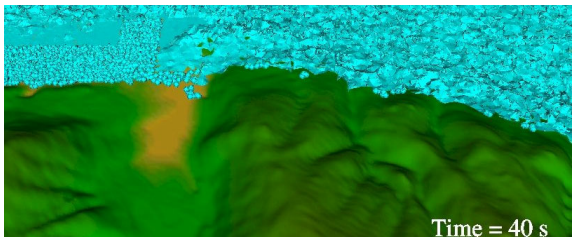

(a)

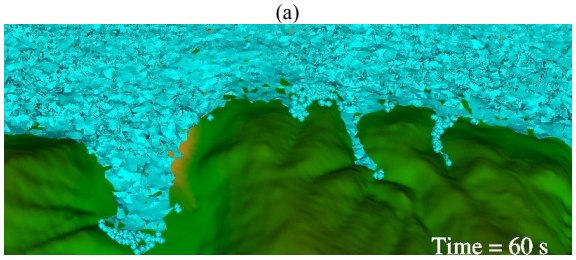

(b)

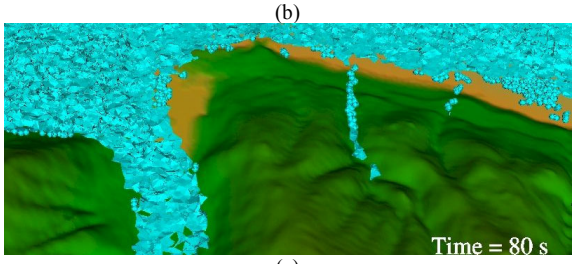

(c)

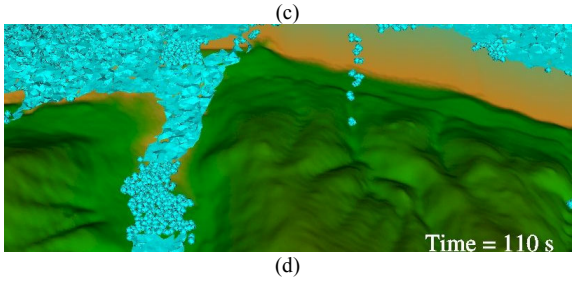

(d)

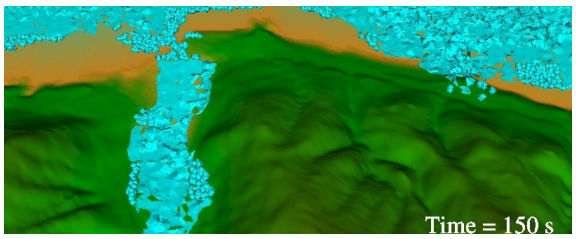

(e)

Figure 3: Back view snapshots of the predicted inundation of the coastline by the tsunami wave at different times

Figure 4 shows the variation in the kinetic, potential and total energy of the fluid, summed over all fluid particles. The vertical axis represents the energy in joules and the horizontal axis represents time in seconds. The total energy here is the sum of the potential and kinetic energies. As the wave-maker pushes the fluid both the kinetic and potential energy of the fluid increase sharply. The kinetic energy reaches a maximum of around $3.2x10^{13}$ J after 5 s when the wave-maker reaches its maximum velocity. The potential energy reaches a maximum of approximately $4x10^{13}$ J after 10 s of simulation when the wave-maker stops pushing the fluid. As time progresses the potential energy of the fluid decreases as it is converted into kinetic energy. After around 110 s the kinetic energy exceeds the potential energy. At this time both have a value of around $1.5x10^{13}$ J. The potential energy continues to gradually decline to a negligible value at around 200 s. The kinetic energy remains stable at around $1.5x10^{13}$ J from 50 to 150 s before starting to decrease gradually. This energy is contained in the increasingly number of smaller and less coherent waves resulting from multiple reflections of the complex coastal topography and interaction with the shoaling sea floor. Eventually viscous dissipation would damp out all these waves.

Figure 5 shows the variation in the average wave speed of the tsunami wave with time. The average wave speed was taken as the velocity obtained from the average kinetic energy of the fluid particles. The wave speed peaks around 15 m/s or 54 km/h at 5 s when the wave-maker is at its peak speed. It then declines to around 10 m/s after 50 s and remains stable at that value until 150 s. After that the wave speed again starts falling and reaches a value of around only 8 m/s at 200 s.

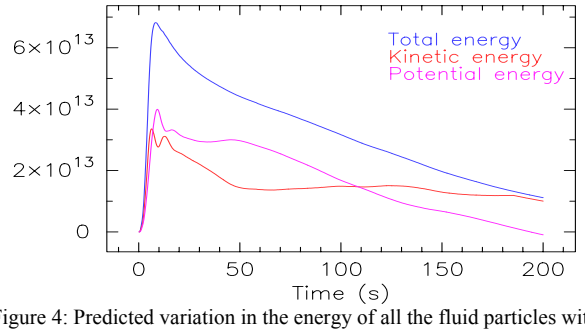

Figure 4: Predicted variation in the energy of all the fluid particles with time.

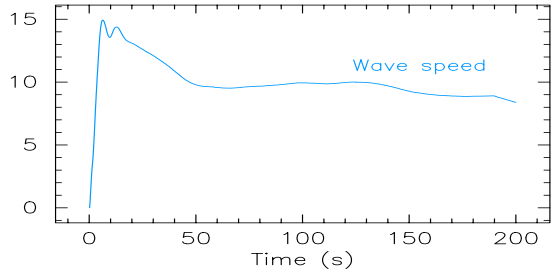

Figure 5: Predicted variation in the average wave speed (in m/s) with time. The average is over all fluid particles.

This simulation takes approximately 60 hrs of CPU time for 200 s of simulation time, using a single 500 MHz processor on a COMPAQ ES40. Although we have not yet carried out any comparisons with measured data for such types of simulations, the above exercise gives reasonable levels of confidence that SPH can be used to solve real scale geophysical problems with relative ease. The next step is to examine the effect of changes in coastal topography and assessing the effect of tsunamis with different intensities and orientations relative to the coast. In the above simulations the use of a 10 m spatial resolution was sufficient to resolve wave and inundation behaviour for this 50 m high wave. This was found to be true for another similar geophysical application carried out by the authors [12]. However, most tsunami events for which quantitative data exists are smaller waves and will require a finer spatial resolution to enable us to make quantitative comparisons. These are long but feasible simulations.

Conclusions

The paper presents the use of SPH for simulating tsunamis on real three-dimensional topography. The results obtained from the simulations suggest that SPH can simulate a tsunami wave with interactions with the surrounding topography including wave propagation, splashing, preferential inundation, wave refraction and break up. The next step in our study will assess the effect of tsunamis with different orientations and intensities with an aim to compare them with real tsunami data. This will give confidence in SPH as a useful tool for assessing the effect of a tsunami. Once an acceptable level of confidence is achieved, SPH can be used as a valuable tool for the prediction of these waves and can prove to be extremely useful in minimising the loss of life and property.

References

[1] Mercado, A. & McCann W., Numerical simulation of the 1918 Puerto Rico Tsunami., *Natural Hazards*, **18**, 1998, 57-76.

[2] Piatanesi, A., Tinti, S. & Bortolucci, E., Finite-Element simulations of the 28 December 1908 Messina Straits (Southern Italy) Tsunami., *Phys. Chem. Earth (A)*, **24**, 1999, 145-150.

[3] Tinti, S., Bortolucci, E. & Romagnoli C., Computer simulation of Tsunami due to sector collapse at Stromboli, Italy., *J of Vol. & Geo. Res.*, **96**, 2000, 103-128.

[4] Gingold, R.A. & Monaghan, J.J., Smoothed particle hydrodynamics. Theory and application to non-spherical stars., *Mon. Not. Roy. Astron. Soc.*, **181**, 1977, 375-389.

[5] Monaghan, J.J., Simulating free surface flows with SPH, *J. Comp. Phys.*, **110**, 1994, 399-406.

[6] Cleary, P., High pressure die casting simulations with SPH: Isothermal single fluid flow., *Proc. Chemeca 97, Paper FL3B on CD Rom*, 1997.

[7] Ha, J., Cleary, P., Alguine, V. and Nguyen, T., Simulation of die filling in gravity die casting using SPH and MAGMAsoft., Proc. 2nd *Int. Conf. on CFD in Minerals & Processe Ind.*, Melbourne, Australia, 1999, 423-428.

[8] Monaghan, J.J., Smoothed particle hydrodynamics., *Ann. Rev. Astron. Astrophys.*, **30**, 1992, 543-574.

[9] Cleary, P., Ha, J. & Sawley, M., Modelling industrial fluid flow applications using SPH., *Proc. IWBL'99*, 1999.

[10] Cleary, P., New implementation of viscosity: tests with Couette flows. *SPH Technical Note 8, CSIRO DMS, Technical Report DMS – C 96/32*, 1996.

[11] USGS web address: http://www-socal.wr.usgs.gov/north/topo.html

[12] Prakash, M., Debroux, F. & Cleary, P., Three-dimensional modelling of dam-break induced flows using smoothed particle hydrodynamics. *14th Australasian Fluid Mechanics Conference, Adelaide, Australia, 2001.*